A Supplementary Information: Polarisation of water under thermal fields: the effect of the molecular dipole and quadrupole moments

Aidan Chapman and Fernando Bresme, Department of Chemistry Imperial College London

The main paper can be accessed with the DOI: 10.1039/D2CP00756H

A.1 Ensuring Charge Neutrality

Because the electric fields and potentials are calculated from the charge profiles averaged over the simulation trajectories, they can often have deviations away from their expected behaviour for charge neutral systems under periodic boundary conditions, i.e. the total electric field is zero across the box and the potential is zero at the box edges. This deviation gets worse for the potential which is a double integral of the charge profile and the error accumulates, resulting in a linear 'background' error. This is corrected by removing the value of the potential calculated at the rightmost half of the simulation box, weighted by the position along the box, namely the correction,

$$\Delta\phi_{\text{corr}}(z) = \phi_{\text{uncorr}}(L_z)\frac{z}{L_z}, \tag{A.1}$$

where L_z is the simulation box length and $\phi_{\text{uncorr}}(z)$ is the uncorrected surface potential profile. This correction has been applied to all potentials and electric fields presented in this paper. A similar procedure can be done to the electric field by removing the net electric field across the simulation box from the potential profile.

A.2 Appendix: Procedure for Finding Points of Inversion

In order to find the temperatures of inversion, we fitted the thermally induced potential as a function of temperature around its (global) minimum to a second order polynomial of the form,

$$\phi(T) = G(T - T_0)^2 + \phi_0, \tag{A.2}$$

where T_0 is the temperature corresponding to the minimum of the potential, ϕ_0 is the value of the potential at theis temperature and G. The curvature, G, and T_0 were both constrained to be positive in the fitting procedures.

The bin with the nearest temperature to the value of T_0 was then chosen to be the inversion temperature. Properties within this bin are then taken to be the properties at inversion. The average inversion points found were included in main text (Figure 4) if a clear inversion was found in all repeats. Due to this strict criteria, rebinning the data affected the number of inversion points found, as well as their location slightly. The latter is due to the coarsening of the temperature values due to the larger bins. The smoother data from using the larger bin width tended to find a more accurate, if less precise, location of inversion.

The Figures A.1(a)-(d) below show the average fitting parameters obtained compared to the averaged ϕ vs T plots, for each isobar that showed inversion.

A.3 Appendix: Rotation of quadrupole moment densities

The coordinate system we use is illustrated in Figure A.2. Only two angles are used to describe the orientation, because the orientation of the azimuthal angle (rotation of the molecule about the z axis) is averaged out, with no effect on the z coordinates of the atoms in the molecule.

The symmetry of the simulation box means that rotations of molecules about the z axis (azimuth) angle will have no effect on the average, angles are evenly distributed. Using this symmetry the orientations of molecules can be described with 2 angles, the rotation of the dipole moment from the z-axis and the subsequent rotation of the molecular plane about the z-axis.

If the water molecule initially lies in the $y-z$ plane with the dipole moment pointing in the z direction with the origin being an arbitrary point along the z axis (the principal symmetry axis of the molecule), then the rotation of the dipole moment θ can be described with a rotation matrix for a rotation about the y axis [1],

$$R_y(\theta) = \begin{bmatrix} \cos\theta & 0 & \sin\theta \\ 0 & 1 & 0 \\ -\sin\theta & 0 & \cos\theta \end{bmatrix} \tag{A.3}$$

This is applied to the positions of the atoms in the water molecule orientated initially as described above, tilting the molecule away from the z axis.

The second rotation to apply is rotation about the new dipole moment direction by the angle χ. Rotation of a vector about an arbitrary axis,$\mathbf{k}$, can be achieved using the formula [1],

$$\mathbf{v}_{\text{rot}} = \mathbf{v}\cos\chi + (\mathbf{k}\times\mathbf{v})\sin\chi + \mathbf{k}\,(\mathbf{k}\cdot\mathbf{v})(1-\cos\chi). \tag{A.4}$$

Applying these two transformations to the atom positions in each molecule with the definition eq. (9) of the main text gives the result eq. (14) from the main text.

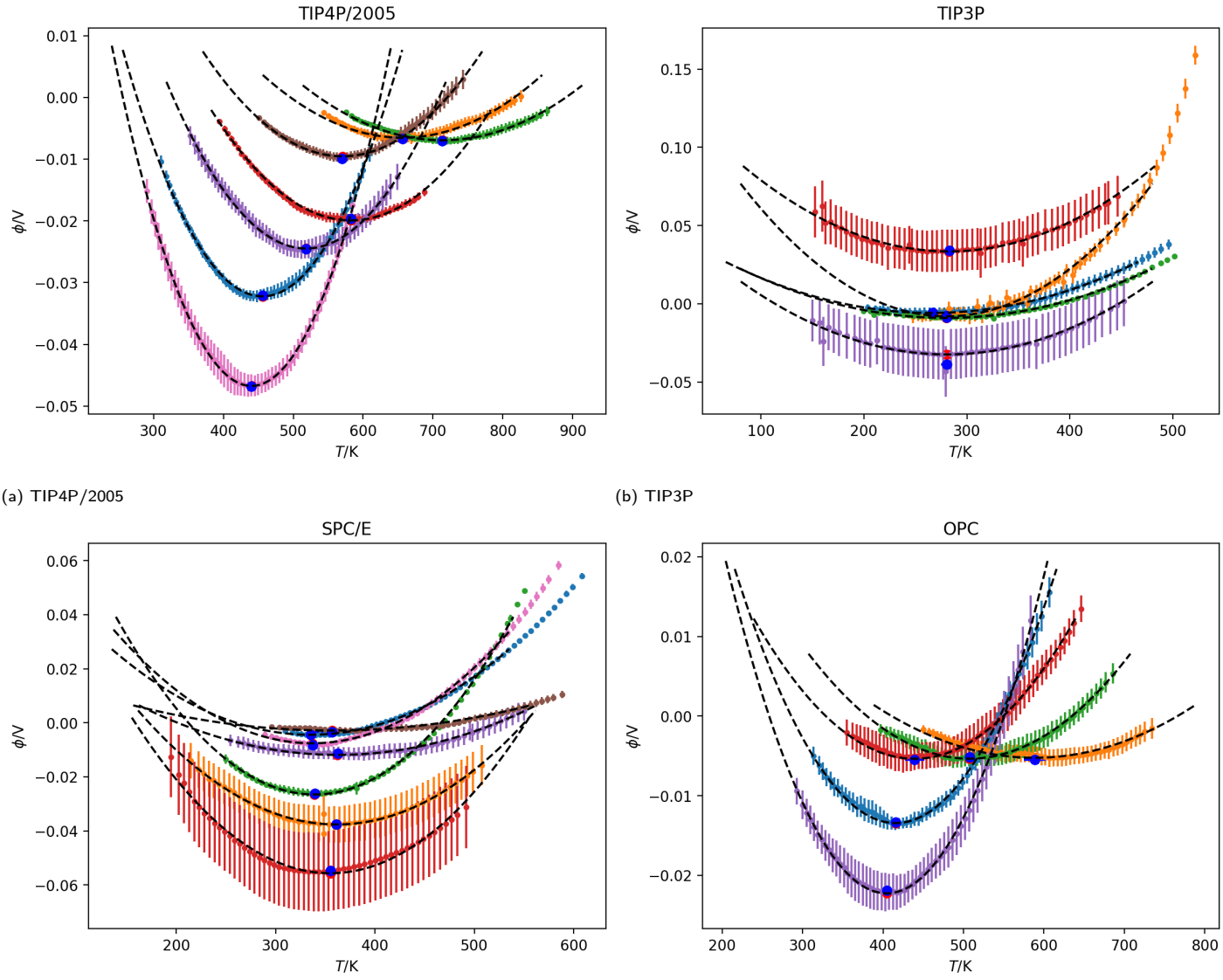

(a) TIP4P/2005

(b) TIP3P

(c) SPC/E

(d) OPC

Fig. A.1 Dotted lines: Plots from averaging fitting parameters for each repeat. Points: Potentials averaged from repeats for each state that showed inversion.

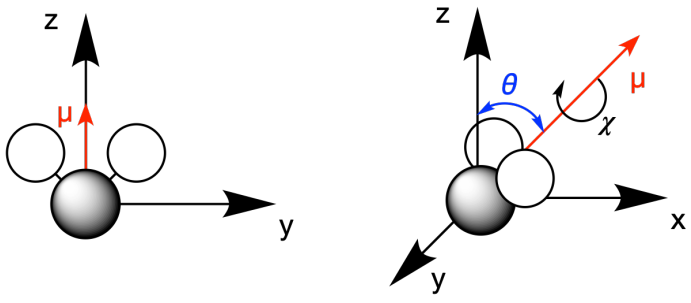

Fig. A.2 Cartoon illustrating the coordinate system for deriving orientation. The left figure illustrates the molecule with an initial orientation of $\theta = 0$, $\chi = 0$. The figure on the right is after orientation, by rotating first about θ, then about χ.

A.4 States investigated in thermopolarisation simulations

			N_{runs}	T	T_{err}	ρ	T_{hot}	$T_{\text{hot,err}}$	T_{cold}	$T_{\text{cold,err}}$	∇T	∇T_{err}	p	p_{err}	T_{inv}	$T_{\text{inv,err}}$	ρ_{inv}	$\rho_{\text{inv,err}}$
TIP4P/2005	250	1021	5	2.586e+02	5.563e-01	1.027e+00	4.277e+02	2.410e-01	7.077e+01	2.749e-01	-4.207e+00	1.010e-02	1.119e+03	1.989e+01	–	–	–	–
	440	940	4	4.310e+02	9.281e-02	9.415e-01	6.144e+02	1.104e-01	2.589e+02	8.849e-02	-4.053e+00	2.203e-03	9.902e+02	8.389e-01	4.400e+02	3.528e+00	9.430e-01	2.923e-03
	460	960	5	4.537e+02	1.579e-01	9.587e-01	6.341e+02	3.118e-01	2.796e+02	2.643e-02	-4.100e+00	2.503e-03	1.731e+03	2.676e+00	4.560e+02	2.682e+00	9.628e-01	2.057e-03
	500	1000	5	4.945e+02	3.141e-01	9.973e-01	6.733e+02	2.508e-01	3.211e+02	8.227e-02	-4.148e+00	2.441e-03	3.552e+03	6.198e+00	5.180e+02	2.710e+00	9.834e-01	2.056e-03
	540	1040	8	5.362e+02	1.890e-01	1.037e+00	7.126e+02	1.077e-01	3.627e+02	3.917e-02	-4.182e+00	2.045e-03	5.892e+03	4.097e+00	5.825e+02	2.736e+00	1.010e+00	1.664e-03
	575	1080	11	5.713e+02	1.733e-01	1.077e+00	7.811e+02	3.450e+01	4.170e+02	1.783e+01	-4.208e+00	6.071e-03	8.555e+03	7.127e+01	–	–	–	–
	590	1100	11	5.878e+02	3.316e-01	1.097e+00	7.963e+02	3.502e+01	4.335e+02	1.865e+01	-4.228e+00	2.853e-03	1.007e+04	5.319e+01	–	–	–	–
	600	990	11	5.903e+02	1.596e+00	9.875e-01	8.801e+02	5.526e+01	4.784e+02	2.925e+01	-4.099e+00	1.006e-02	5.143e+03	1.003e+02	5.699e+02	6.437e+00	1.000e+00	4.050e-03
	690	1020	12	6.794e+02	2.136e+00	1.018e+00	1.008e+03	6.215e+01	5.976e+02	3.586e+01	-4.021e+00	4.688e-02	8.379e+03	9.365e+01	6.567e+02	8.037e+00	1.029e+00	4.629e-03
	720	1040	12	7.147e+02	9.541e-01	1.037e+00	1.041e+03	6.388e+01	6.340e+02	3.836e+01	-4.086e+00	3.042e-02	1.020e+04	4.072e+01	7.134e+02	6.035e+00	1.037e+00	2.896e-03
	900	300	5	8.439e+02	1.419e-01	2.920e-01	1.078e+03	3.753e-01	7.062e+02	1.230e-01	-2.786e+00	3.796e-03	5.874e+02	3.881e-01	–	–	–	–
		1100	5	8.997e+02	5.086e-01	1.098e+00	1.071e+03	2.259e-01	7.265e+02	2.309e-01	-4.192e+00	5.307e-03	1.881e+04	1.140e+01	–	–	–	–
	1200	300	5	1.183e+03	1.245e+00	2.973e-01	1.384e+03	3.039e-01	1.010e+03	3.611e-01	-2.869e+00	6.300e-03	1.483e+03	2.624e+00	–	–	–	–
	1300	300	5	1.286e+03	6.693e-01	2.978e-01	1.485e+03	5.583e-01	1.110e+03	7.870e-02	-2.866e+00	7.861e-03	1.741e+03	1.264e+00	–	–	–	–
	1500	300	5	1.493e+03	9.357e-01	2.985e-01	1.685e+03	5.517e-01	1.312e+03	2.121e-01	-2.840e+00	4.608e-03	2.237e+03	1.789e+00	–	–	–	–
		400	5	1.491e+03	1.173e+00	3.982e-01	1.684e+03	3.414e-01	1.313e+03	4.676e-01	-3.130e+00	6.059e-03	3.296e+03	3.792e+00	–	–	–	–
		500	5	1.494e+03	8.288e-01	4.980e-01	1.682e+03	4.284e-01	1.314e+03	3.714e-01	-3.366e+00	6.432e-03	4.714e+03	3.497e+00	–	–	–	–
		750	5	1.498e+03	2.324e-01	7.481e-01	1.679e+03	3.406e-01	1.319e+03	1.905e-01	-3.793e+00	5.242e-03	1.095e+04	2.435e+00	–	–	–	–
		1000	5	1.501e+03	4.748e-01	9.983e-01	1.673e+03	4.184e-01	1.324e+03	2.236e-01	-4.094e+00	8.114e-03	2.481e+04	8.263e+00	–	–	–	–
		1100	5	1.502e+03	4.964e-01	1.098e+00	1.671e+03	3.065e-01	1.328e+03	2.300e-01	-4.172e+00	4.434e-03	3.407e+04	1.048e+01	–	–	–	–
		1270	5	1.502e+03	1.874e-01	1.269e+00	2.500e+03	5.258e-01	2.000e+03	4.900e-01	-4.267e+00	5.147e-03	5.725e+04	6.966e+00	–	–	–	–
SPC/E	340	1000	5	3.401e+02	2.671e-01	1.004e+00	5.156e+02	1.901e-01	1.606e+02	1.115e-01	-4.159e+00	2.006e-03	1.108e+03	1.097e+01	3.553e+02	2.476e+00	1.007e+00	1.590e-03
	360	1020	5	3.578e+02	2.290e-01	1.022e+00	5.346e+02	1.442e-01	1.807e+02	4.760e-02	-4.171e+00	2.522e-03	1.765e+03	3.461e+00	3.612e+02	3.305e+00	1.028e+00	2.243e-03
	400	930	5	3.926e+02	2.641e-01	9.294e-01	5.739e+02	1.251e-01	2.183e+02	5.184e-02	-4.072e+00	3.626e-03	3.924e+02	2.894e+00	3.396e+02	1.309e+00	9.860e-01	8.493e-04
		1060	5	4.007e+02	1.041e-01	1.057e+00	5.739e+02	9.594e-02	2.216e+02	4.467e-02	-4.233e+00	1.880e-03	3.538e+03	1.354e+00	3.625e+02	9.448e+00	1.083e+00	5.692e-03
	440	940	5	4.289e+02	3.481e-01	9.409e-01	6.142e+02	2.310e-01	2.588e+02	8.246e-02	-4.066e+00	5.166e-03	1.103e+03	4.803e+00	3.375e+02	6.627e+00	1.017e+00	4.114e-03
		1100	5	4.387e+02	1.499e-01	1.097e+00	6.125e+02	1.645e-01	2.630e+02	3.502e-02	-4.255e+00	2.252e-03	5.901e+03	3.461e+00	3.568e+02	1.835e+01	1.144e+00	1.006e-02
	460	960	5	4.515e+02	1.713e-01	9.584e-01	6.342e+02	1.155e-01	2.795e+02	7.079e-02	-4.109e+00	2.189e-03	1.822e+03	2.000e+00	3.351e+02	7.123e+00	1.046e+00	3.922e-03
	475	1140	5	4.746e+02	1.856e-01	1.137e+00	6.464e+02	1.587e-01	2.996e+02	4.368e-02	-4.281e+00	2.077e-03	8.730e+03	4.368e+00	–	–	–	–
	490	1160	5	4.905e+02	2.249e-01	1.156e+00	6.611e+02	8.942e-02	3.153e+02	8.733e-02	-4.305e+00	1.732e-03	1.027e+04	5.897e+00	–	–	–	–
	500	1000	5	4.939e+02	2.069e-01	9.972e-01	6.736e+02	2.177e-01	3.210e+02	7.157e-02	-4.152e+00	3.182e-03	3.585e+03	3.904e+00	–	–	–	–
		1050	5	4.958e+02	1.670e-01	1.047e+00	6.728e+02	1.923e-01	3.223e+02	1.005e-01	-4.205e+00	2.644e-03	5.264e+03	3.263e+00	–	–	–	–
	540	1040	5	5.356e+02	1.848e-01	1.037e+00	7.127e+02	1.927e-01	3.623e+02	8.538e-02	-4.188e+00	2.158e-03	5.790e+03	3.538e+00	–	–	–	–
	575	1080	5	5.708e+02	1.187e-01	1.077e+00	7.471e+02	1.249e-01	3.986e+02	8.254e-02	-4.221e+00	3.384e-03	8.342e+03	2.489e+00	–	–	–	–
	590	1080	5	5.857e+02	6.318e-02	1.077e+00	7.618e+02	2.776e-01	4.138e+02	9.078e-02	-4.212e+00	3.470e-03	8.723e+03	1.344e+00	–	–	–	–
		1100	5	5.878e+02	7.192e-02	1.097e+00	7.617e+02	2.223e-01	4.145e+02	1.584e-01	-4.232e+00	3.799e-03	9.744e+03	2.131e+00	–	–	–	–
	600	990	5	5.929e+02	1.628e-01	9.875e-01	7.733e+02	2.440e-01	4.214e+02	1.066e-01	-4.128e+00	2.932e-03	5.299e+03	3.228e+00	–	–	–	–
	620	1100	5	6.176e+02	1.528e-01	1.097e+00	7.915e+02	1.881e-01	4.446e+02	1.471e-01	-4.234e+00	3.131e-03	1.054e+04	3.390e+00	–	–	–	–
	720	1040	5	7.165e+02	3.947e-01	1.037e+00	8.922e+02	1.471e-01	5.436e+02	6.776e-02	-4.159e+00	2.405e-03	9.995e+03	8.056e+00	–	–	–	–
TIP3P	200	1270	5	2.080e+02	1.062e-01	1.271e+00	3.721e+02	1.327e-01	2.453e+01	3.172e-02	-4.441e+00	1.988e-03	8.042e+03	1.577e+01	–	–	–	–
	260	1096	5	2.616e+02	1.291e-01	1.097e+00	4.342e+02	1.731e-01	8.123e+01	9.072e-02	-4.278e+00	5.841e-03	2.291e+03	9.960e+00	–	–	–	–
	300	992	5	2.973e+02	9.086e-02	1.007e+00	4.745e+02	1.244e-02	1.198e+02	8.154e-02	-4.172e+00	2.217e-03	7.655e+02	4.911e+00	2.803e+02	5.127e+00	1.033e+00	3.546e-03
		995	5	2.949e+02	1.786e-01	9.992e-01	4.748e+02	2.098e-01	1.195e+02	5.573e-02	-4.132e+00	2.509e-03	5.982e+02	7.269e+00	2.827e+02	1.957e+00	1.024e+00	1.379e-03
		1100	5	3.004e+02	7.929e-02	1.097e+00	4.737e+02	1.011e-01	1.211e+02	9.766e-02	-4.274e+00	2.364e-03	3.013e+03	6.081e+00	–	–	–	–
	350	992	5	3.445e+02	1.647e-01	1.004e+00	5.239e+02	2.065e-01	1.699e+02	4.337e-02	-4.167e+00	2.685e-03	1.430e+03	2.546e+00	2.805e+02	3.282e+00	1.060e+00	2.115e-03
		993	5	3.439e+02	1.234e-01	9.918e-01	5.238e+02	1.071e-01	1.693e+02	2.186e-02	-4.138e+00	1.428e-03	1.172e+03	1.971e+00	2.666e+02	7.770e+00	1.059e+00	4.890e-03
		1200	5	3.518e+02	1.366e-01	1.195e+00	5.211e+02	1.817e-01	1.744e+02	2.101e-02	-4.337e+00	2.644e-03	8.457e+03	4.754e+00	–	–	–	–
	400	873	5	3.672e+02	2.344e-01	8.836e-01	5.648e+02	5.237e-01	2.154e+02	6.044e-02	-3.751e+00	4.145e-03	-1.148e+01	2.400e+00	2.801e+02	6.055e+00	9.930e-01	4.953e-03
		992	5	3.928e+02	9.833e-02	1.002e+00	5.734e+02	9.740e-02	2.201e+02	4.149e-02	-4.170e+00	2.874e-03	2.272e+03	1.762e+00	–	–	–	–
		1200	5	4.002e+02	9.351e-02	1.196e+00	5.705e+02	2.257e-01	2.253e+02	6.747e-02	-4.332e+00	3.362e-03	1.006e+04	3.110e+00	–	–	–	–
	440	840	5	4.017e+02	2.989e-01	8.463e-01	6.027e+02	1.956e-01	2.545e+02	5.619e-02	-3.700e+00	6.069e-03	1.033e+02	3.310e+00	–	–	–	–
	470	860	5	4.447e+02	2.758e-01	8.618e-01	6.416e+02	2.098e-01	2.863e+02	9.231e-02	-3.892e+00	1.885e-03	7.368e+02	3.633e+00	–	–	–	–
	500	880	5	4.816e+02	2.062e-01	8.776e-01	6.734e+02	2.041e-01	3.173e+02	8.550e-02	-3.980e+00	1.947e-03	1.450e+03	3.003e+00	–	–	–	–
		1151	5	4.976e+02	2.504e-01	1.147e+00	6.709e+02	1.611e-01	3.250e+02	6.334e-02	-4.297e+00	2.620e-03	1.041e+04	7.084e+00	–	–	–	–
	550	870	5	5.322e+02	1.350e-01	8.679e-01	7.236e+02	1.568e-01	3.676e+02	1.033e-01	-3.955e+00	2.857e-03	2.052e+03	2.142e+00	–	–	–	–
	580	1500	5	5.820e+02	2.300e-01	1.498e+00	7.419e+02	6.938e-02	4.159e+02	5.028e-02	-4.421e+00	3.615e-03	5.315e+04	1.095e+01	–	–	–	–
	590	900	5	5.763e+02	2.405e-01	8.974e-01	7.645e+02	1.959e-01	4.089e+02	5.915e-02	-4.012e+00	9.662e-04	3.275e+03	2.982e+00	–	–	–	–
	610	900	5	5.974e+02	4.018e-01	8.973e-01	7.841e+02	1.202e-01	4.292e+02	4.398e-02	-4.014e+00	2.492e-03	3.622e+03	6.554e+00	–	–	–	–
	625	920	5	6.163e+02	2.147e-01	9.155e-01	7.989e+02	2.463e-01	4.447e+02	5.388e-02	-4.048e+00	5.111e-03	4.360e+03	2.993e+00	–	–	–	–
	650	910	5	6.387e+02	1.694e-01	9.073e-01	8.243e+02	9.901e-02	4.698e+02	1.099e-01	-4.030e+00	3.948e-03	4.544e+03	2.601e+00	–	–	–	–
	800	1211	5	7.998e+02	3.916e-01	1.208e+00	9.691e+02	1.887e-01	6.282e+02	1.836e-01	-4.298e+00	3.341e-03	2.438e+04	1.066e+01	–	–	–	–
OPC	440	940	5	4.321e+02	1.675e-01	9.408e-01	6.117e+02	1.539e-01	2.615e+02	6.877e-02	-3.994e+00	3.039e-03	8.562e+02	2.842e+00	4.047e+02	1.979e+00	9.678e-01	1.368e-03
	460	960	5	4.543e+02	2.404e-01	9.584e-01	6.312e+02	9.516e-02	2.823e+02	5.926e-02	-4.034e+00	2.422e-03	1.651e+03	3.900e+00	4.161e+02	5.452e+00	9.891e-01	3.615e-03
	500	1000	5	4.956e+02	1.233e-01	9.973e-01	6.705e+02	1.591e-01	3.239e+02	3.079e-02	-4.073e+00	9.570e-04	3.636e+03	2.203e+00	4.393e+02	1.194e+01	1.033e+00	7.069e-03
	540	1040	8	5.371e+02	1.749e-01	1.037e+00	7.097e+02	9.396e-02	3.657e+02	6.836e-02	-4.103e+00	2.009e-03	6.190e+03	3.985e+00	5.078e+02	5.737e+00	1.053e+00	3.068e-03
	575	1080	8	5.717e+02	1.736e-01	1.078e+00	7.434e+02	1.143e-01	4.021e+02	9.306e-02	-4.121e+00	3.155e-03	9.188e+03	4.364e+00	–	–	–	–
	590	1100	8	5.885e+02	1.951e-01	1.097e+00	7.578e+02	1.390e-01	4.180e+02	1.241e-01	-4.135e+00	4.716e-03	1.085e+04	5.100e+00	5.890e+02	1.377e+01	1.097e+00	6.255e-03
	600	990	10	5.941e+02	1.409e-01	9.877e-01	7.701e+02	1.007e-01	4.245e+02	6.910e-02	-4.041e+00	2.177e-03	5.449e+03	3.089e+00	–	–	–	–
	690	1020	10	6.854e+02	1.705e-01	1.018e+00	8.594e+02	1.241e-01	5.161e+02	1.016e-01	-4.057e+00	3.290e-03	8.933e+03	3.667e+00	–	–	–	–
	720	1040	8	7.174e+02	2.041e-01	1.037e+00	8.887e+02	2.315e-01	5.472e+02	9.520e-02	-4.071e+00	1.723e-03	1.077e+04	4.785e+00	–	–	–	–
	1500	1270	5	1.504e+03	3.748e-01	1.269e+00	1.662e+03	3.315e-01	1.336e+03	3.564e-01	-4.164e+00	1.059e-02	6.192e+04	1.261e+01	–	–	–	–

Table A.1 Results of inversion simulations. The first two columns indicate the target temperatures and density, respectively. All temperatures have units of K, all densities are in $\mathrm{g/cm^3}$, all temperature gradients are in units of $\mathrm{K/\AA}$ and all pressures are in atmospheres. T_{hot} and T_{cold} are the averages of the hot and cold thermostatting regions over the course of the simulations and over the separate replicas. All quantities with an 'inv' suffix are inversion properties and all quantities with 'err' are the standard errors of the corresponding property, calculated from the repeats.

A.5 Checking Linear Response

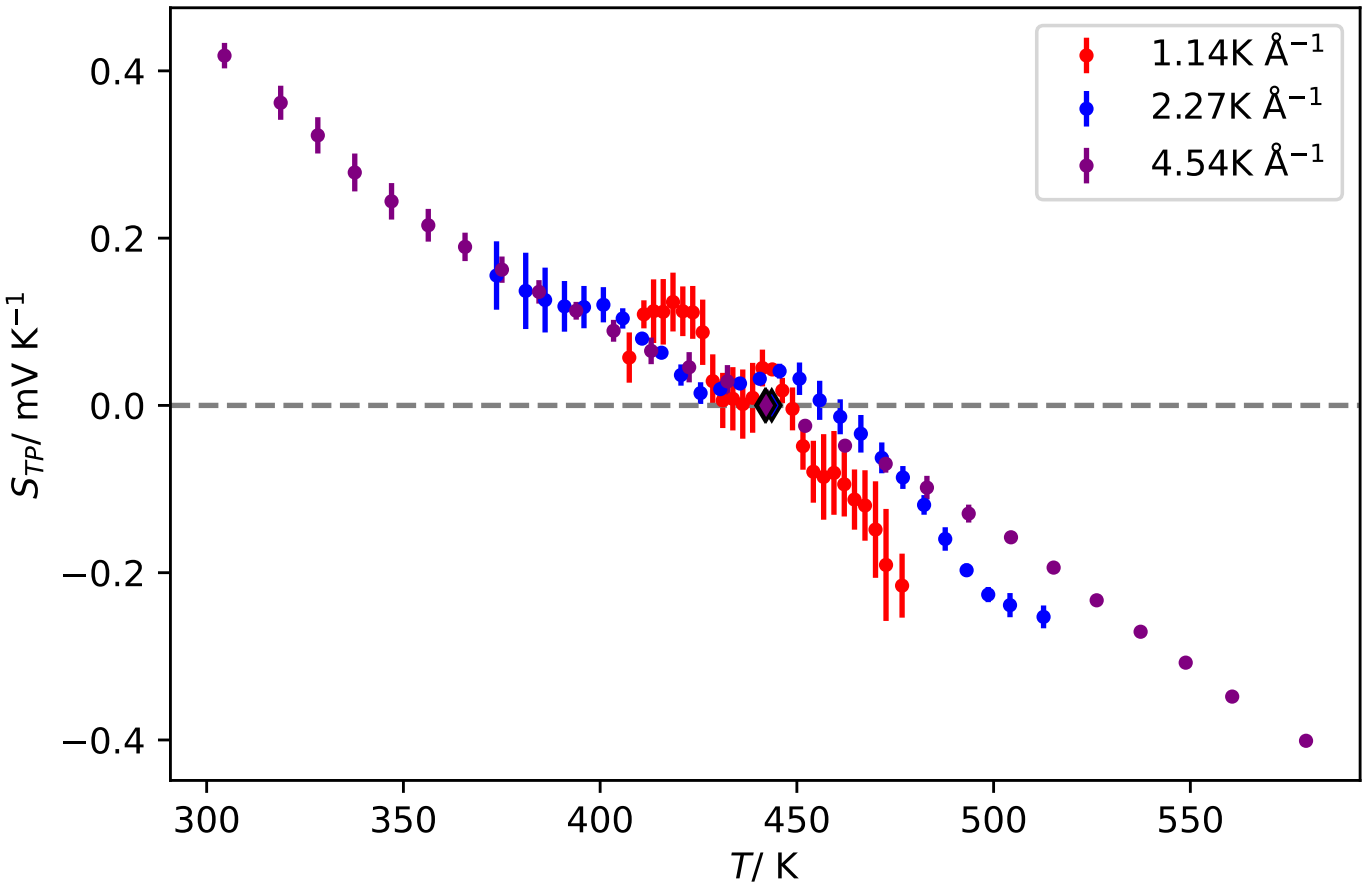

Fig. A.3 Verification of the invariance with temperature gradient of the thermopolarisation coefficient for the state with target temperature and density of 440 K and 0.94 g/cm^3, using the TIP4P/2005 model. To get the different thermal gradients (shown in the legend), the hot and cold thermostats were set to 100 K, 200 K and 300 K above and below the average temperature. Re-binning to 2.5 Å was applied here to make the profiles smoother. The large amount of noise in the 1.14 K/Å system can be attributed to the flatter thermal gradient giving rise to more noise. More sampling would be required to accurately reproduce the S_{TP} coefficient of higher thermal gradients. The diamond points indicate the points of inversion, which are very close for all 3 gradients.

A.6 Pressure Profiles

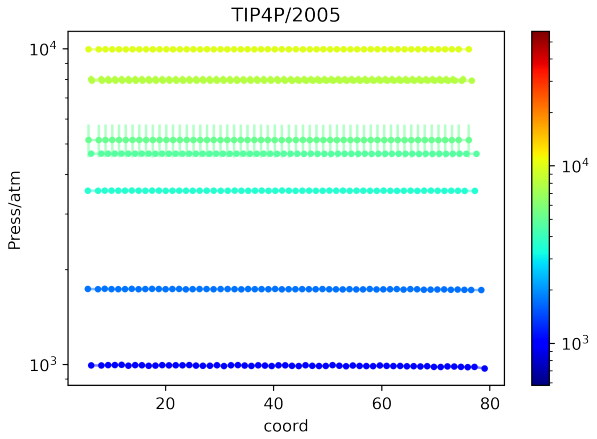

(a) TIP4P/2005

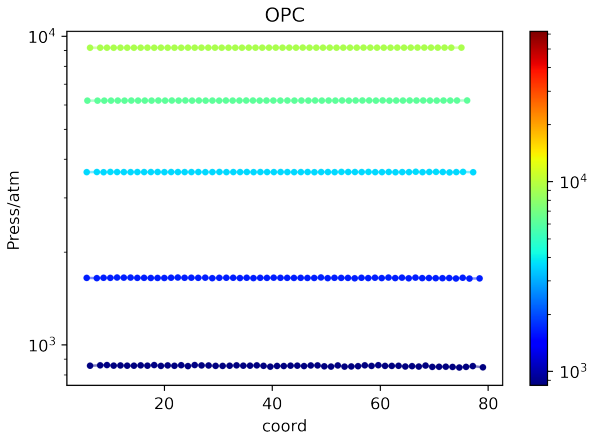

(b) OPC

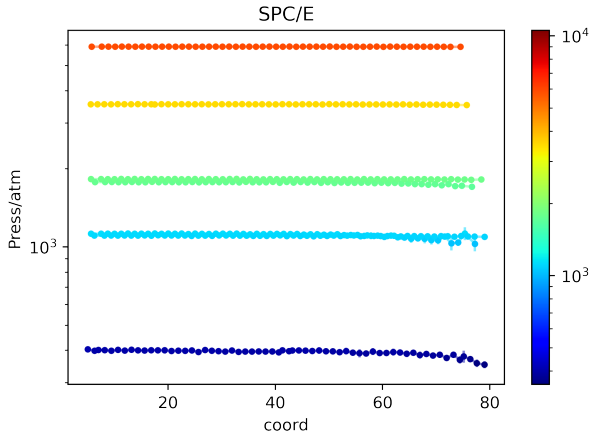

(c) SPC/E

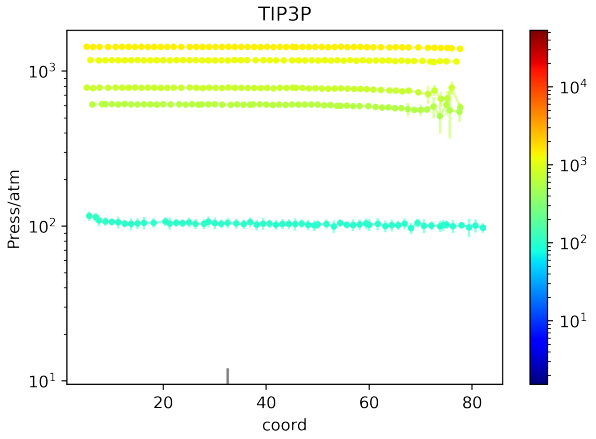

(d) TIP3P

Fig. A.4 Local pressure profiles across the NEMD simulations boxes for isobars that show inversion. Lines are coloured by the pressure, given in atmospheres.

A.7 Comparison Between NEMD and Equation of States

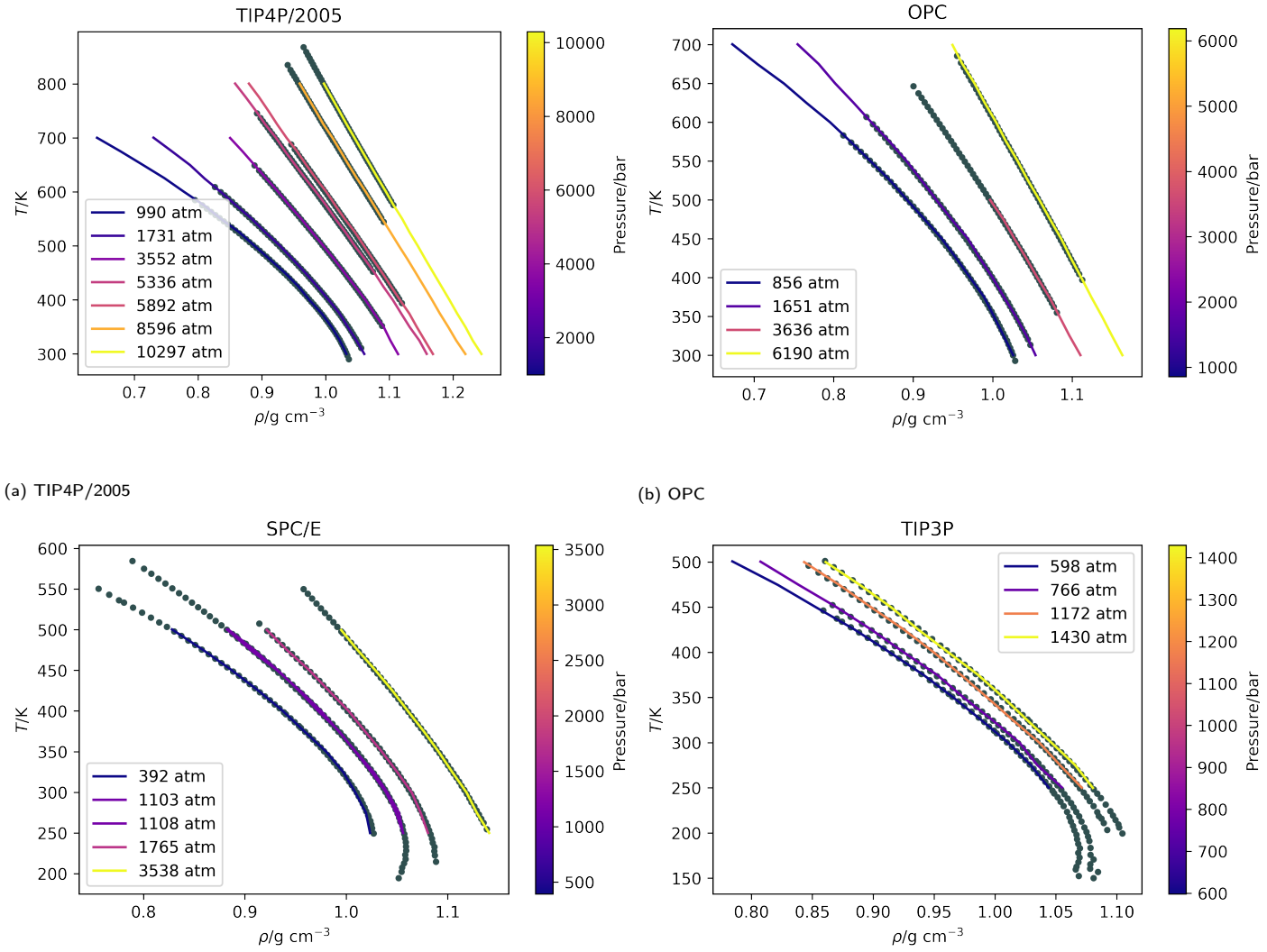

(a) TIP4P/2005

(b) OPC

(c) SPC/E

(d) TIP3P

Fig. A.5 Equations of state from NEMD simulations (points) compared to corresponding isobars from equilibrium (NpT) simulations (lines). The equilibrium simulations were performed with 2 fs timestep for 10^5 steps of equilibration and 10^5 production. No tail corrections were used, to be consistent with the pressure calculated from the stress profile of NEMD simulations.

A.8 TIP3P Orientation Profiles at Low Temperature

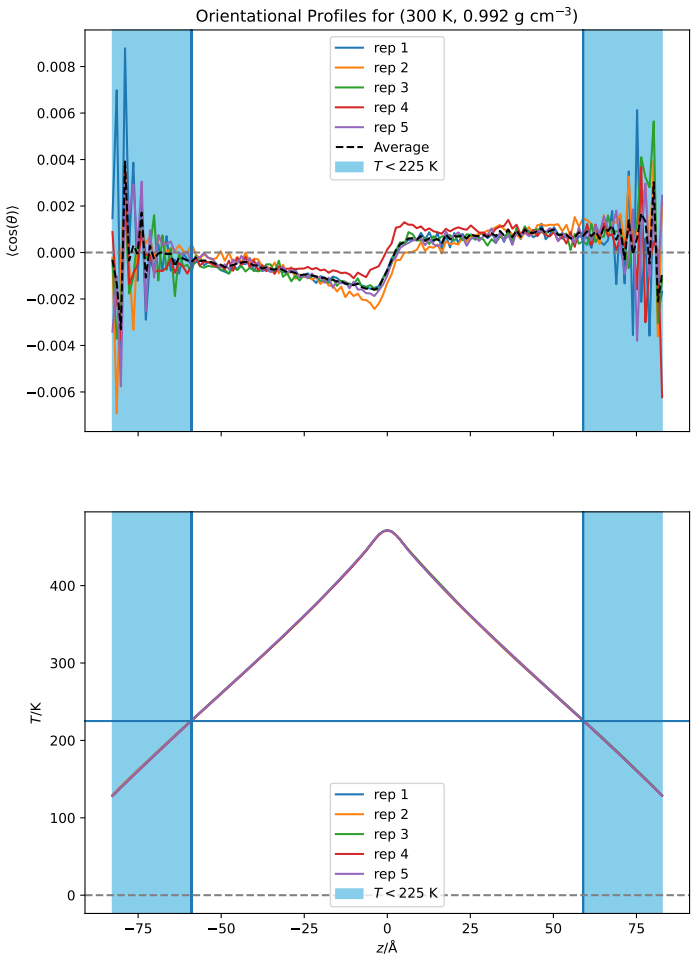

Fig. A.6 Orientation profile of TIP3P water for 5 repeats, each of 2 ns each. The orientation remains smooth apart from toward the cold regions at the edges of the box, where there is substantial noise in the orientation. These profiles have all been shifted so the angle at the edges is zero.

A.9 Verification of the Inversion Criteria

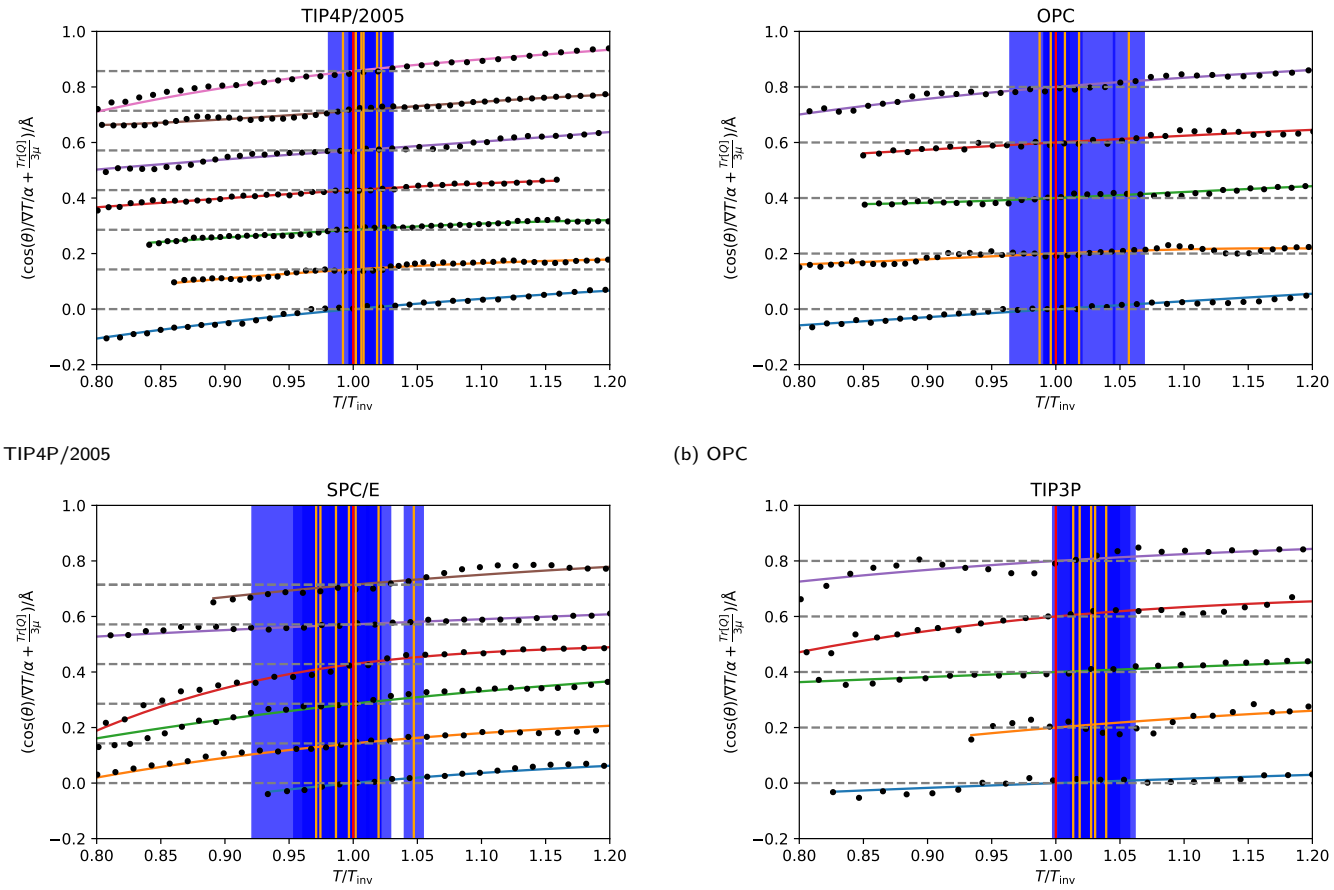

(a) TIP4P/2005

(b) OPC

(c) SPC/E

(d) TIP3P

Fig. A.7 Checking the alternative inversion criteria presented in equation (28) in the main text. The solid curves are spline fittings used to find the roots where inversion occurs. The spline fittings are applied to the data sets for with an extra 5 bin rolling average applied. The temperature axis is scaled relative to the temperature of inversion found by this criterion. The orange vertical lines are the temperatures of inversion found by the quadratic fittings, with the blue shaded regions being the corresponding errors. The lines for each state have been offset in the y-axis for visual clarity, the dotted grey lines indicating where zero is. The $(T,\ \rho) = (440\,\text{K},\ 1.1\,\text{g/cm}^3)$ state for the SPC/E model is not shown here, the spline fit did not yield a root, due the inversion region occurring near the edge of the box with a large amount of noise.

Table A.2 Parameters from fitting the LV density profiles of the OPC model, without long range corrections

	ρ_0	ρ_v	K	L	$\rho_{0,err}$	$\rho_{v,err}$	K_{err}	L_{err}
300	0.988666	1.563735e-04	0.769459	49.826833	0.000181	2.981999e-05	0.009858	0.006646
350	0.965644	3.362332e-11	0.633839	51.037580	0.000182	3.479845e-11	0.006089	0.011312
400	0.931387	1.699284e-06	0.513650	52.912770	0.000246	3.799714e-06	0.004101	0.016831
425	0.910770	7.000902e-05	0.468803	54.099424	0.000106	1.274440e-04	0.004374	0.013064
450	0.887445	6.594068e-04	0.418733	55.454126	0.000355	1.778928e-04	0.009684	0.007857
475	0.861654	1.540057e-03	0.378413	57.013184	0.000193	1.211963e-04	0.009442	0.011836
500	0.832676	2.944549e-03	0.330634	58.830992	0.000315	2.496384e-04	0.016113	0.030048
525	0.800124	5.393290e-03	0.296354	60.922595	0.000285	3.250234e-04	0.008749	0.029237

Table A.3 Parameters from fitting the LV density profiles of the OPC model, with long range corrections

	ρ_0	ρ_v	K	L	$\rho_{0,err}$	$\rho_{v,err}$	K_{err}	L_{err}
300	0.994539	4.934816e-05	0.746890	49.543558	0.000219	5.221384e-05	0.007222	0.014809
350	0.971261	1.823950e-12	0.579832	50.749358	0.000143	1.797350e-12	0.016951	0.007681
400	0.937359	1.139181e-12	0.490930	52.582267	0.000155	1.653587e-12	0.025696	0.003769
425	0.917202	3.903724e-05	0.416691	53.731108	0.000173	8.728989e-05	0.017618	0.014303
450	0.894486	3.872195e-04	0.408909	55.047668	0.000188	1.475747e-04	0.015605	0.009446
475	0.869355	1.154597e-03	0.341045	56.551884	0.000634	2.973906e-04	0.033646	0.019220
500	0.840600	2.799415e-03	0.325160	58.293384	0.000281	2.238024e-04	0.024890	0.022224

A.10 OPC Coexsitence line

The direct coexistence line of the OPC model of water has not yet been reported. Here we present such a diagram. The densities of the liquid and vapour phases for each temperature the liquid vapour interface were obtained from fittings of the mass density profile to the following function,[2]

$$\rho(z) = \rho_v + \rho_0 \left(1 + \tanh(K(L - |z|))\right), \tag{A.5}$$

ρ is the mass density, ρ_v is the vapour mass density, ρ_0 is the bulk liquid density, K is inversely proportional to the width of the interface and L is the z coordinate of the interface. For the above fitting to work, the z origin is taken to be the centre of the simulation box. All parameters were restricted to be strictly positive.

As well as the LV simulations performed as discussed in the main text, we also performed LV simulations of the OPC with Ewald summation (PPPM) on the dispersion interactions. The accuracy thresholds used for the dispersion interactions were 0.0001 and 0.002 for the real and reciprocal space contributions.

Figure A.8 shows the results from the fittings and Tables A.2 and A.3 show the average parameters from the fittings for the cut-off and full potentials respectively.

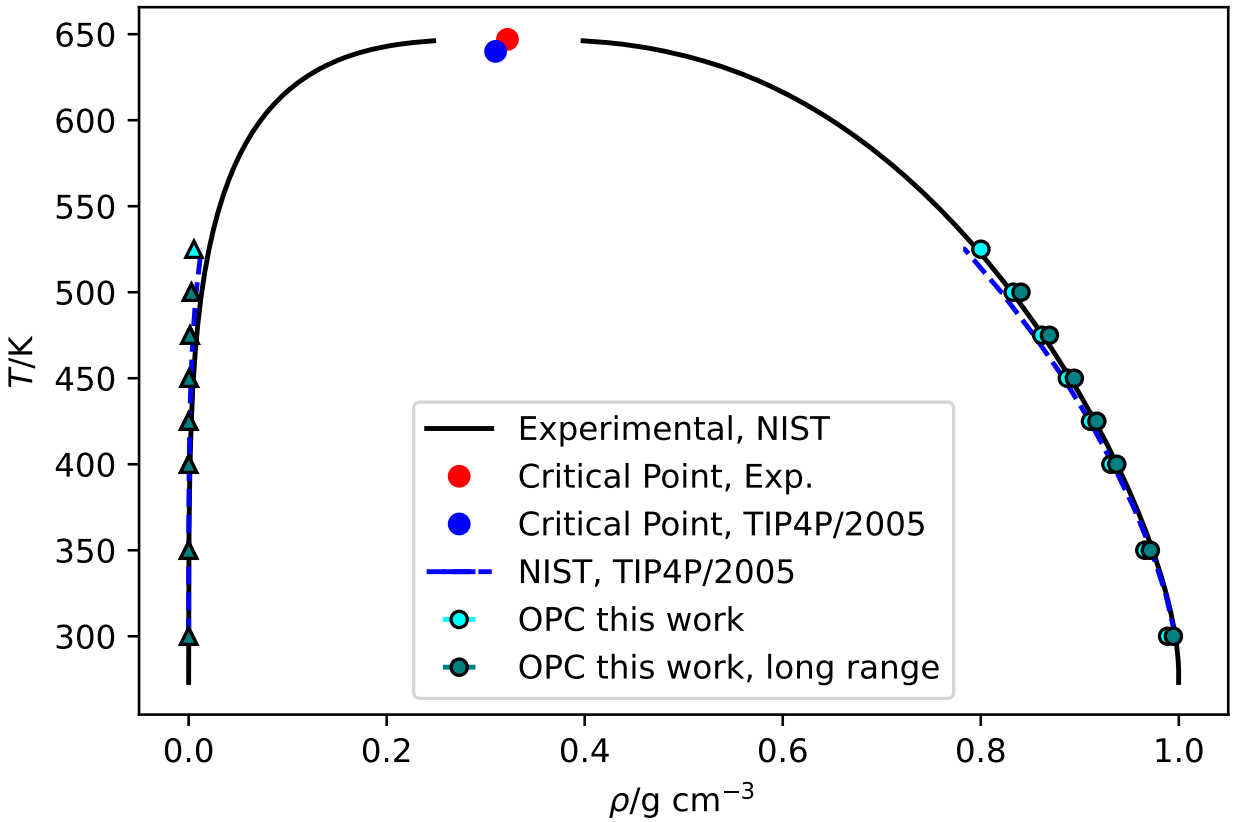

Fig. A.8 Points: liquid and vapour densities found by fitting the OPC liquid vapour density profiles to equation (A.5). Dashed lines: The coexistence lines for the TIP4P/2005 model from NIST[3], provided for comparison. The solid black lines are the experimental saturation curves, also from NIST[4], which are based on the IAPWS-95 equation of state for water.[5]

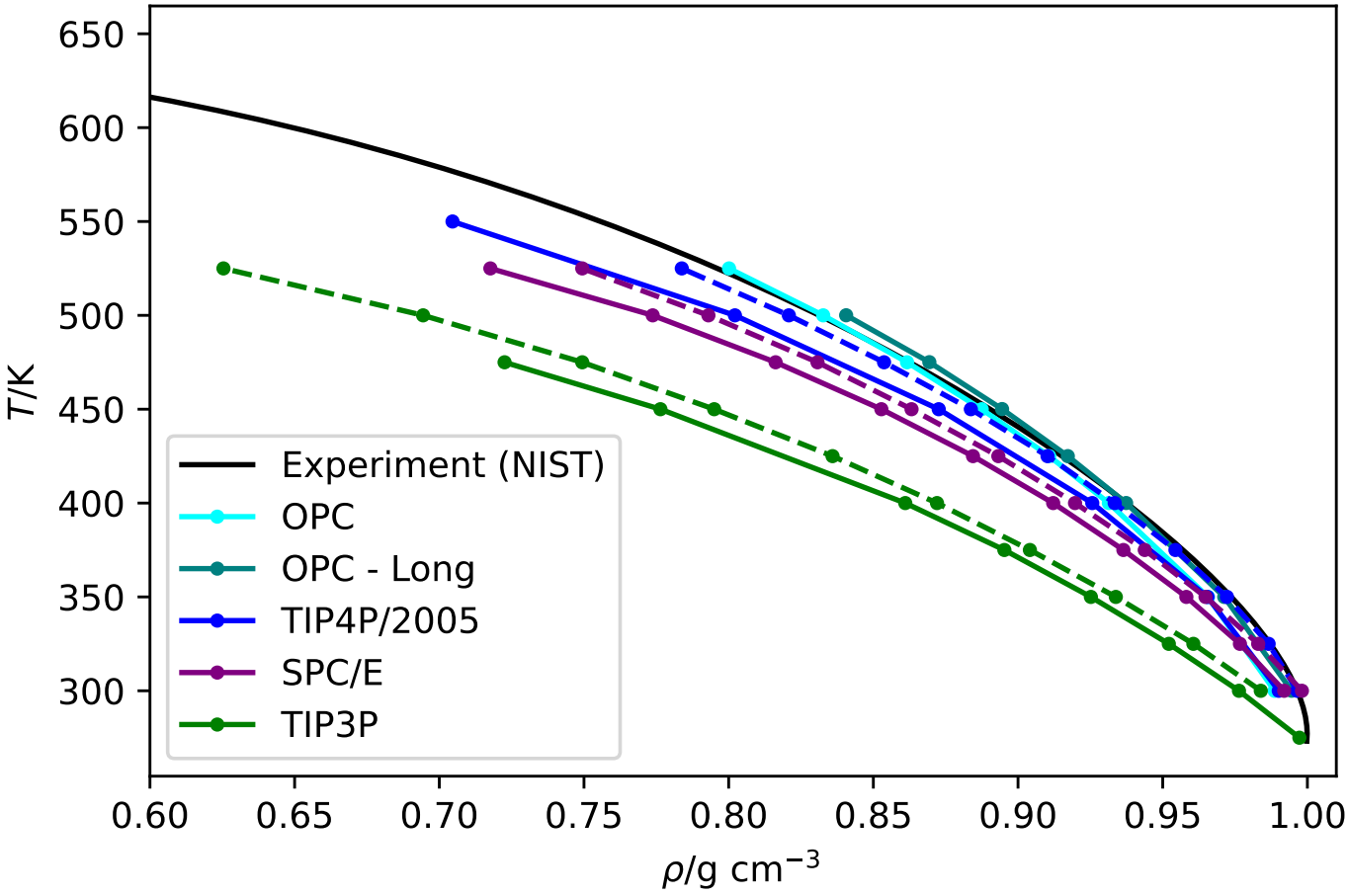

Fig. A.9 Comparison between the various coexistence lines. Dashed lines are from NIST[3], which have tail corrections applied, the solid lines are those calculated in this work. The solid black line is the experimental saturation curve, also from NIST[4], which are based on the IAPWS-95 equation of state for water.[5]

A.11 Results of TIP4P/2005f Simulations

ρ	T	P	d_{OH}	d_{HH}	$H\hat{O}H$	d_{OM}	μ	μ/Q_T	S_{TP}	λ
997.1±0.5	300.5±0.3	-3.8±21	0.09664	0.15301	104.68	0.01555	2.3245	0.9908	0.640±0.330	0.911±0.010
996.8±1	326.0±0.7	247.2±15	0.09654	0.15284	104.67	0.01555	2.3217	0.9918	0.471±0.062	0.920±0.010
994.9±0.9	351.1±0.8	486.6±24	0.09651	0.15274	104.62	0.01555	2.3225	0.9935	0.268±0.042	0.955±0.011
994.6±0.9	401.3±0.9	1338.6±10	0.096435	0.15256	104.56	0.01555	2.3222	0.9957	0.186±0.028	0.975±0.010
995.8±0.9	441.4±1	2161.3±32	0.096395	0.15245	104.51	0.01553	2.3289	0.9972	0.077±0.026	0.987±0.014
993.2±0.7	499.8±1	3285.4±15	0.096365	0.15234	104.45	0.01553	2.3256	0.9992	-0.005±0.016	1.040±0.010

Table A.4 Simulated thermodynamic states for the TIP4P/2005f model/. ρ is the mass density (kg/m^3), T the temperature (K), P pressure in bar, d_{OH} average intramolecular distance between OH (nm), d_{HH} average intramolecular distance between HH (nm), d_{OM} distance oxygen-virtual site (nm), μ dipole moment (Debyes), μ/Q_T dipole-quadrupole ratio Å^{-1}, S_{TP} thermal-polarization coefficient (mV/K) and λ, thermal conductivity (W/(K m)). The hot and cold thermostat temperatures. were set ± 50 K above and below the average temperatures. Additional simulations performed with an average density of $0.940\,\mathrm{g/cm^3}$ and thermostat temperatures of $340\,\mathrm{K}$ and $540\,\mathrm{K}$ in order to capture the temperature of inversion within a single simulation.

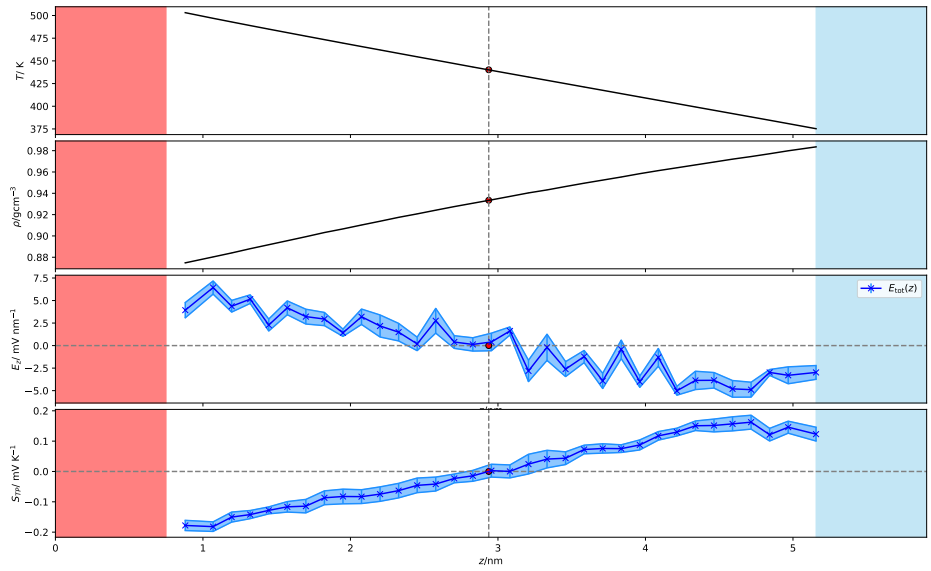

Fig. A.10 Average half box profile for the simulation with average density $0.940\,\mathrm{g/cm^3}$ and thermostat temperatures of $340\,\mathrm{K}$ and $540\,\mathrm{K}$. The blue and red shaded regions represent the removed thermostatting regions of $340\,\mathrm{K}$ and $540\,\mathrm{K}$. The red markers highlight the point inversion for E_z and S_{TP}.

References

1 M. L. Boas, *Mathematical Methods in the Physical Sciences*, Wiley, 3rd edn, 2005.

2 E. Harder and B. Roux, *J. Chem. Phys.*, 2008, **129**, 234706.

3 V. Shen, D. Siderius, W. Krekelberg and H. Hatch, *NIST Standard Reference Simulation Website, NIST Standard Reference Database Number 173*, accessed June 2022, https://www.nist.gov/programs-projects/nist-standard-reference-simulation-website.

4 E. W. Lemmon, I. H. Bell, M. L. Huber and M. O. McLinden, *Thermophysical Properties of Fluid Systems, NIST Chemistry WebBook, NIST Standard Reference Database Number 69*.

5 W. Wagner and A. Pruß, *Journal of Physical and Chemical Reference Data*, 2002, **31**, 387–535.